





RESEARCH ARTICLE | JANUARY 19 2024

Resilience of transportation infrastructure networks to road failures

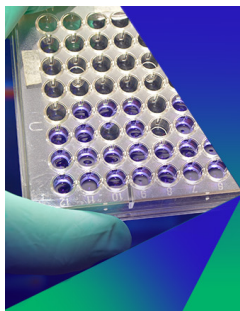
Special Collection: [Nonlinear dynamics, synchronization and networks: Dedicated to Jürgen Kurths' 70th birthday](#)

Jonas Wassmer   ; Bruno Merz  ; Norbert Marwan 

 Check for updates

Chaos 34, 013124 (2024)

<https://doi.org/10.1063/5.0165839>



Biomicrofluidics

Special Topic:
Microfluidics and Nanofluidics in **India**

Submit Today



Resilience of transportation infrastructure networks to road failures

Cite as: Chaos 34, 013124 (2024); doi: 10.1063/5.0165839
Submitted: 30 June 2023 · Accepted: 28 November 2023 ·
Published Online: 19 January 2024



View Online



Export Citation



CrossMark

Jonas Wassmer,^{1,a)} Bruno Merz,^{2,b)} and Norbert Marwan^{3,c)}

AFFILIATIONS

¹Institute of Environmental Science and Geography, University of Potsdam, 14476 Potsdam, Germany

²German Research Centre for Geosciences (GFZ), 14473 Potsdam, Germany

³Potsdam Institute for Climate Impact Research (PIK), Member of the Leibniz Association, 14473 Potsdam, Germany

Note: This paper is part of the Focus Issue on Nonlinear dynamics, synchronization and networks: Dedicated to Juergen Kurths' 70th birthday.

a) Author to whom correspondence should be addressed: jonas.wassmer@pik-potsdam.de. Also at: Potsdam Institute for Climate Impact Research (PIK), 14473 Potsdam, Germany.

b) Also at: Institute of Environmental Science and Geography, University of Potsdam, 14476 Potsdam, Germany.

c) Also at: Institute of Geosciences, University of Potsdam, 14476 Potsdam, Germany and Institute of Physics and Astronomy, University of Potsdam, 14476 Potsdam, Germany.

ABSTRACT

Anthropogenic climate change drives extreme weather events, leading to significant consequences for both society and the environment. This includes damage to road infrastructure, causing disruptions in transportation, obstructing access to emergency services, and hindering humanitarian organizations after natural disasters. In this study, we develop a novel method for analyzing the impacts of natural hazards on transportation networks rooted in the gravity model of travel, offering a fresh perspective to assess the repercussions of natural hazards on transportation network stability. Applying this approach to the Ahr valley flood of 2021, we discovered that the destruction of bridges and roads caused major bottlenecks, affecting areas considerably distant from the flood's epicenter. Furthermore, the flood-induced damage to the infrastructure also increased the response time of emergency vehicles, severely impeding the accessibility of emergency services. Our findings highlight the need for targeted road repair and reinforcement, with a focus on maintaining traffic flow for emergency responses. This research provides a new perspective that can aid in prioritizing transportation network resilience measures to reduce the economic and social costs of future extreme weather events.

© 2024 Author(s). All article content, except where otherwise noted, is licensed under a Creative Commons Attribution (CC BY) license (<http://creativecommons.org/licenses/by/4.0/>). <https://doi.org/10.1063/5.0165839>

To ensure that every individual can be reached by emergency services in time, it is crucial to ensure the functionality of the road network. This becomes particularly important to follow natural disasters, which often result in deterioration of the road infrastructure due to road damage. Consequently, traffic is rerouted locally, which creates bottlenecks that affect the dynamics of the system on a large scale. We propose a novel method using a traffic-based centrality measure based on the gravity model of travel to analyze the impacts of natural hazards on the transportation infrastructure, specifically focusing on traffic flow stability. As a case study, we analyze the aftermath of the flood disaster in the Ahr valley, where the road infrastructure was severely compromised.

I. INTRODUCTION

The growing frequency and severity of extreme weather events driven by anthropogenic climate change lead to an increasing amount of negative consequences on both human societies and natural ecosystems.^{1,2} Among others, they can result in substantial deterioration of road infrastructure and the impairment of critical components such as bridges or tunnels. As a consequence, traffic flows can be disrupted,³ hindering the passage of ambulances, fire trucks, and other emergency vehicles. Disturbance in infrastructure networks can also lead to obstructions in supply chains and commerce, ultimately causing a decrease in productivity and economic output.⁴ Thus, the consequences of extreme weather events on road networks extend beyond transportation and can have severe

impacts on public safety, emergency services, and humanitarian aid organizations.^{5,6}

This was demonstrated alarmingly during the devastating flood event that hit the Ahr valley in Germany in 2021. The importance of resilient infrastructure was illustrated during the devastating flooding in Western Europe in July 2021 that caused 46 billion damage. The Ahr catchment, a rather small tributary of the Rhine, was particularly hard hit; 134 people died in the Ahr valley.⁷ The flash floods severely damaged the transportation infrastructure, resulting in the destruction of almost all bridges.⁸ This caused critical bottlenecks that impeded rescue efforts and hindered access to assistance for a significant portion of the population.⁹

These impacts, along with an increasing risk for extreme weather events, highlight the need for improved disaster preparedness and mitigation measures, such as effective planning, design, and construction of roads and transportation infrastructure. Infrastructure planning has to take into account the potential impacts of natural disasters on roads to minimize their negative consequences and to ensure the continued functioning of essential transportation systems.

In this study, we aim to better understand the impacts of extreme weather events on road networks and, consequently, the operational capability of emergency services. With this goal in mind, we examine the resilience of road networks to flood-induced damage concerning traffic flow. To accomplish this, we develop a method that allows us to simulate the traffic dynamics and impairments after the flood. Using this method, we aim to identify key road network components that require special protective measures to enhance stability as part of disaster preparedness strategies.

Prior research on the effects of natural disasters on road networks has centered around assessing impaired connectivity through the utilization of centrality measures.¹⁰ Building upon these approaches, subsequent research has explored the accessibility of emergency services during natural disasters by utilizing centrality indicators such as betweenness and closeness centrality to assess connectivity, as well as isochrones to measure accessibility.¹¹ Moreover, betweenness centrality has been employed as an indicator to evaluate the criticality of road infrastructure, aiding in the development of preparedness and mitigation strategies for ensuring continued access to healthcare services in disaster situations.¹² Additionally, the resilience of road networks has been investigated in terms of traffic delays resulting from congestion caused by road closures. The findings indicate that many urban transportation networks are resilient against disruptions.¹³

In this paper, we examine the impact of flood-induced alterations on the topology of road infrastructure networks and how such changes influence traffic dynamics. Specifically, we investigate the emergence of bottlenecks following the local closure of roads, which have the potential to disrupt traffic flow on a large scale. Utilizing a traffic-based centrality measure, our analysis quantifies the resilience of the road network under post-flood conditions in terms of traffic flow. Additionally, we explore the implications of a compromised road network on the efficacy of emergency services' accessibility, an aspect critical to disaster response and recovery.

As a case study, we examine the effects of the Ahr valley flood on the stability and dynamics of the transportation network. We simulate various traffic scenarios in the area impacted by the flood.

By comparing different scenarios in which the system is constrained to varying degrees, we can estimate the additional time spent in congestion and the resulting challenges faced by emergency services due to the disruptions. Additionally, we evaluate the proportion of the population that is affected by the negative impact on emergency accessibility in the affected region. Moreover, we identify roads that significantly impact the stability of the transportation system. To this end, we analyze how the collapsed bridge infrastructure affects the functionality of the road network and measure which bridges have the greatest impact on functionality and are, therefore, candidates for reconstruction as early as possible and for particular protection to safeguard their functioning during future floods. This information can assist policy makers in prioritizing road restoration or reinforcement efforts to mitigate the effects of extreme weather events.

Following the Introduction, we give a theoretical background and methodology section, where we propose our method. Subsequently, we examine the traffic restrictions caused by the Ahr flood as a case study and present our findings in the Results section. Finally, we conclude the paper with a discussion.

II. THEORETICAL BACKGROUND AND METHODS

In this section, we present a novel method to analyze the resilience of traffic flow to flood-induced road failures in roads networks. Our approach combines a comprehensive understanding of the vehicular mobility pattern, the topology of the road network and data from past flood events. To gain a detailed insight in the topology of the road network, we utilize the OpenStreetMap (OSM) data set.¹⁴ Furthermore, we use satellite imagery capturing the extent of the flooding¹⁵ to analyze how the event affected the topology of the network. To simulate vehicular mobility behavior, we analyze survey data on the German mobility patterns¹⁶ as well as population data from the "Global Human Settlement Layer" (GHSL).¹⁷ This comprehensive methodology enables us to obtain a thorough understanding of the impact of a flood event to the infrastructure.

A. Graph representation of the road network

The road network acts as an indispensable backbone for mobility by enabling the transportation of goods and people over long distances. It also plays a crucial role in the urban fabric, managing the daily flow of traffic and thus contributing to social and economic prosperity. In urban areas, a well-designed road network facilitates access to services and resources, which is why great efforts are made to optimize road networks in terms of the traffic flow.^{18,19} A road network can be described as a graph in which the edges represent the roads and the nodes correspond to the intersections and ends of the roads. Because every road, that is not a bridge, intersects another road at a junction, the corresponding graph is inherently planar.²⁰

We obtain the data of the road network from the OSM database, which is a collaborative open-source project that aims to create a free, editable map of the world.¹⁴ Managed by a global community of volunteers, OSM data are used for various applications like transportation planning,¹³ urban analysis,^{21–24} disaster management,^{11,12,25,26} and environmental analysis.^{27,28} It offers

advantages such as detailed and up-to-date information, transparent updates, and an open licence. However, limitations exist due to volunteer-based data collection, leading to potential inconsistencies.

In panel (a) of Fig. 1, we present the historical representation of the Ahr area obtained from OSM, dated January 2021, which was prior to the flood event. This historical data set is sourced from Ref. 29, which provides regularly updated and comprehensive copies of the OSM database. By utilizing the historical data set, we ensure that our modeling captures the condition of the region before any potential impacts caused by the flood event. Furthermore, utilizing the OSM data, we extract hospital facilities in the region [see Fig. 1(a)]. Additionally, we map the footprint of the riverine flooding of the Ahr river that occurred on July 14th and 15th, 2021 in Western Germany. We obtain the flood footprint from the data set “EMSR517: Flood in Western Germany” provided by the “European Copernicus Emergency Management Service” (EMS).¹⁵

To mathematically describe the road network, we define a directed graph denoted by $G(V, E)$, where E represents the collection of directed edges describing road segments connecting vertices V , which represent the set of vertices describing road intersections or end points. Each directed edge, denoted by $\ell = (i \rightarrow j) = (ij) \in E$, connects two nodes i and $j \in V$, representing the directionality of the road segments in the network. Concluding, a one-way street from i to j is represented as a directed edge $(i \rightarrow j)$ in the graph, whereas a two-way street is represented by two directed edges, $(i \rightarrow j)$ and $(j \rightarrow i)$, to account for both directions of travel. To define further

properties of the road network, such as road length $l_{ij} \in \mathbb{R}$ or speed limits $v_{ij, \text{limit}} \in \mathbb{R}$, we introduce weighted edges, where each edge can be associated with multiple values to describe the respective properties. In addition, we can assign properties or attributes to nodes in the graph to describe them as representatives of hospitals or fire stations.

We construct the graph of the road network from OSM using publicly accessible software Osmium³⁰ and OSMnx.³¹ We visualized the graph representation of the road network in panel (b) of Fig. 1.

To assess the impact of flooding on road networks, a range of methodologies can be employed that can be grouped between immediate short-term and persistent long-term effects. Short-term effects could be analyzed by adopting a model that designates roads as inoperative only when water levels exceed a predefined threshold, as indicated in the literature.^{32,33} Until this threshold is reached, roads are considered navigable, albeit with reduced speed. However, in this paper, we do not account for the potential drastic changes in the overall mobility behavior that can occur during or right after severe weather incidents.³⁴ Thus, we aim to understanding how flood-induced road damage alters traffic dynamics over an extended period, i.e., when mobility behavior has returned to normal, but flood-induced road damage is still prevalent.

In a long-term analysis, roads are marked as closed post-event if they sustain damage or are destroyed. We determine this by whether a road intersects with the flood’s extent. We depict the roads that intersect with the flood’s extend in panel (b) of Fig. 1 by color

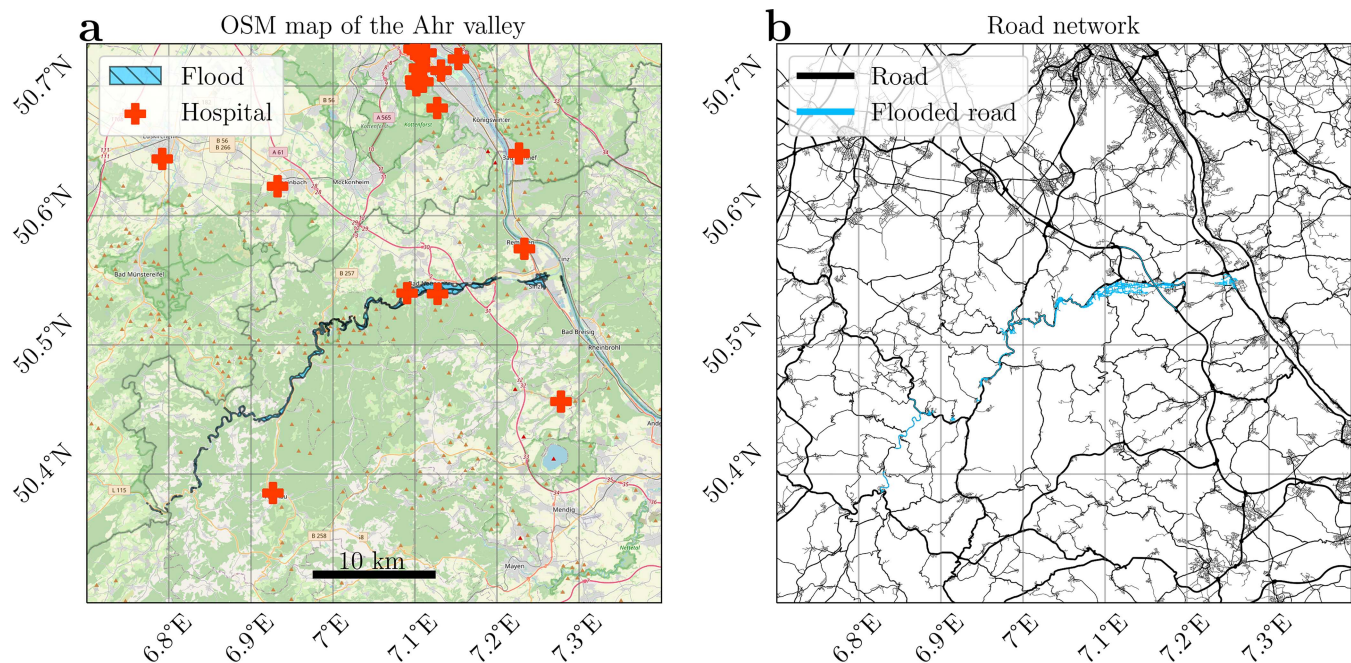


FIG. 1. Using OSM to extract the road network from a selected area (here, we show the Ahr region as an example). (a) Area surrounding the Ahr river in Western Germany, based on OSM (Lat. 6.7°E to 7.4°E and Lon. 50.2°N to 50.75°N). Hospitals are highlighted with red cross symbols. The region affected by the flood is shown as the light blue area. (b) Corresponding road graph $G(V, E)$ extracted from OSM, consisting of 62 106 edges $(ij) \in E$ representing the roads and 26 040 nodes $k \in V$ representing the intersections between two or more roads. We highlight the roads rendered “non-operational” by flooding by color coding them light blue.

coding them light blue. We recognize the inherent simplification in this approach, as it is not a given that all roads within the flood's trajectory will be closed thereafter. A more nuanced assessment could be achieved by acquiring a detailed data set from the relevant authorities, specifying which roads were closed and which remained open.

To mathematically describe the closure of a roads, we remove the set of edges $R \subset E$ that correspond the closed roads from the graph, yielding $G_r(V, E \setminus R)$. This provides an immediate assessment of the impact of the flood on the road network and offers flexibility in adjusting parameters, such as adding or removing more roads, to facilitate further analysis.

B. Mobility in Germany

Understanding the dynamics of drivers' mobility behavior is crucial for an accurate simulation of traffic systems. To investigate this, we draw upon the extensive data set of the German Mobility Panel (MOP),¹⁶ an annual longitudinal study that has been conducted since 1994. It provides insights into the daily mobility behavior in Germany. The MOP collects data through household surveys and examines travel patterns and influencing factors.

To analyze realistic traffic patterns, this section aims to determine the number of vehicles present on the road network at any given time within a specified region. To achieve this, we illustrate in panel (a) of Fig. 2 the distribution of vehicles in the road network throughout the course of a day. The data points are presented as ratios of total daily commuters, ensuring that the sum of all hourly data points adds up to one. The survey shows most travel happens during the day with peaks at 7:00 AM and 5:00 PM due to rush hours. A notable variance in traffic distribution is observed when contrasting weekdays with weekends, as demonstrated in panel (b). The weekday patterns, characterized by significant peaks at the rush hours, sharply contrast with the singular mid-morning peak on Saturdays and the more evenly spread, subdued traffic on Sundays.

In panel (c), our analysis reveals that on weekdays, about 55% of Germany's population employs cars for their daily commutes. On Saturdays, this proportion drops to 45% and on Sundays to 35%. Our analysis further suggests an urban-rural divide in vehicle use. In cities with a well-developed public transportation system, the percentage of private vehicle use tends to be lower, while in rural areas where such facilities are sparse, the reliance on private vehicles is significantly higher. Data supporting this observation, depicted in panel (d), were first collected in 2020, underscoring the influence of population density on transportation preferences.

These findings suggest that transportation behavior and the reliance on private vehicles vary significantly depending on factors such as time of day, day of the week, and population density. In Appendix A 1, we further show that the weather has a slight influence on vehicle usage. The results emphasize the importance of considering such factors in transportation planning to optimize mobility options and to reduce congestion in urban areas while meeting the diverse transportation needs of individuals residing in different regions. In the context of this study, these findings help us determining the occupancy rate of roads in the transportation network. However, it is important to note that this mobility analysis averages out extraordinary events such as natural disasters where

the mobility behavior could be significantly different.³⁴ Thus, in this paper, we aim to analyze the long-term effects of flood-induced damage of the transportation network and we do not aim to mimic the mobility during such an event.

C. From mobility patterns to traffic flow: A macroscopic perspective

In order to model the traffic in a given area, our goal in this section is to estimate the number of vehicles on the road network at different time intervals. For this purpose, we define an occupancy rate $\gamma \in [0, 1]$, which describes the proportion of all vehicles on the road at a given time. By integrating this factor into the traffic model, we aim to simulate a realistic traffic pattern within a given region.

The mobility pattern of an individual is a complex and multifaceted phenomenon that has been the subject of numerous studies in the fields of transportation engineering and urban planning.^{35–37} While individuals do not always takes the shortest paths,^{38,39} it is still widely assumed that they tend to optimize their routing behavior such that their travel time is minimized.^{13,40,41} This assumption is based on the “theory of rational choice,” which posits that people make decisions based on a cost-benefit analysis.⁴² In the context of mobility, the “cost” is associated with the travel time of a route, which travelers try to minimize.⁴³

To analyze the traffic dynamics, there exists a vast selection of traffic simulation models that can be categorized into two categories: macroscopic and microscopic models. Microscopic simulations, although slower to compute, are frequently employed to analyze urban traffic. They enable the examination of both macroscopic and microscopic elements of the system, like encompassing traffic light algorithms. In these simulations, individual entities such as travelers, vehicles, and traffic lights are modeled with great precision.

In contrast, macroscopic simulations are relatively fast and demand less computing power. They concentrate on traffic flow modeling using high-level mathematical models and are well suited for studying extensive systems where detailed modeling is not necessary.⁴⁴

In this study, we are analyzing large systems, and hence, we develop a macroscopic model that uses a traffic-based centrality measure based on the gravity model of travel,^{45,46} which is commonly used to analyze the transportation infrastructure,⁴⁷ aid in evacuation planning,⁴⁸ or improve accessibility of healthcare services.⁴⁹

The gravity model predicts a commuter flow between different locations based on the demand or attractiveness of the given locations. It is based on the idea that the attraction between two locations, in terms of vehicle travel, is similar to the gravitational attraction between two physical objects. This analogy is a simple and intuitive way to understand the factors that influence the flow of people, goods, or capital between different locations, which makes it an efficient way to predict traffic flow.

In this analysis, we employ the relative population size of different locations as a measure of the attractiveness of a region. The underlying assumption is that travelers are more likely to go to areas with larger populations. Additionally, we posit that the level of attraction between two locations diminishes as the travel time between them increases.

Vehicle usage in Germany

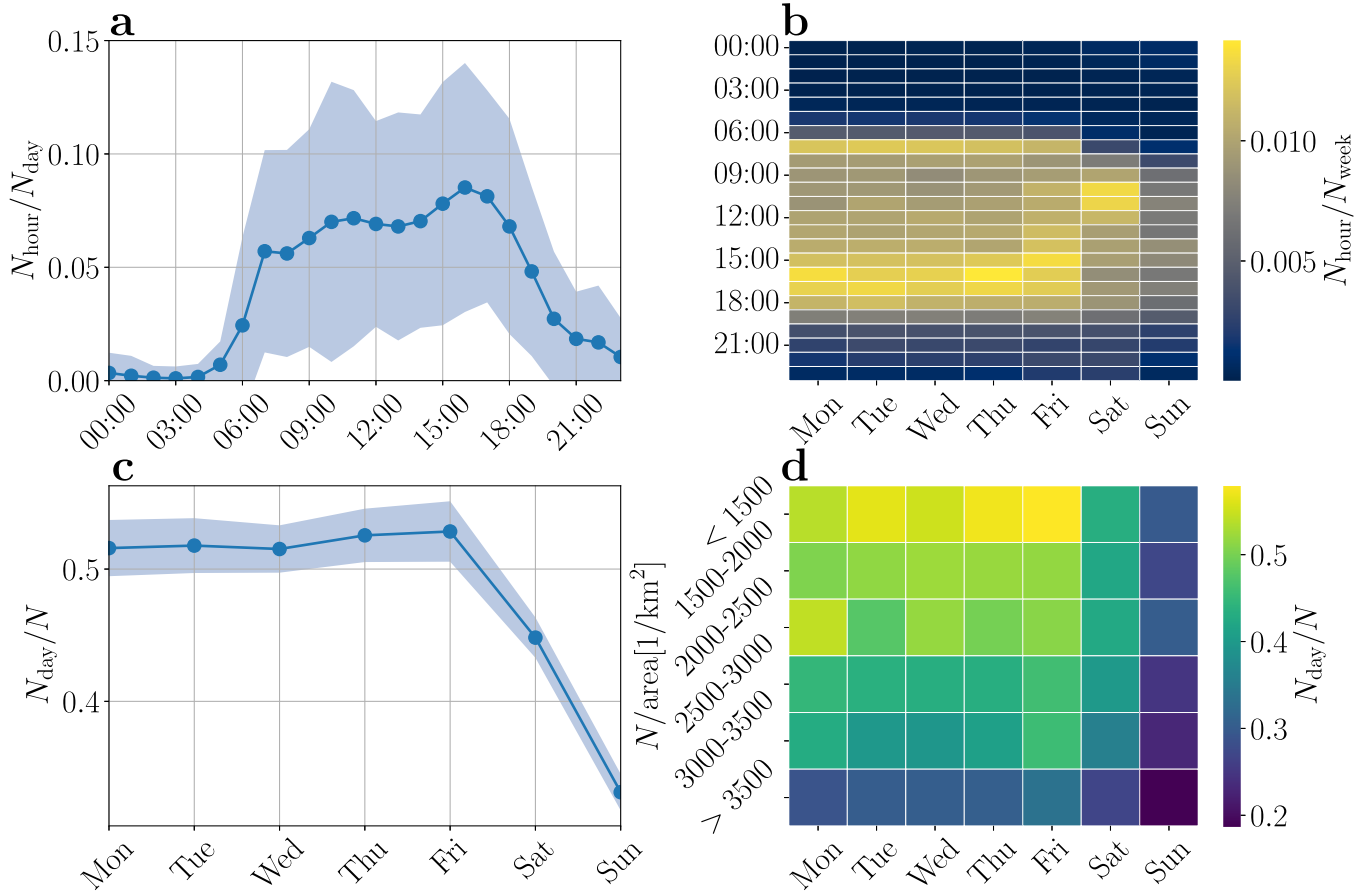


FIG. 2. Daily vehicle usage in Germany based on the German Mobility Panel (MOP).¹⁶ (a) Average percentage distribution of car users throughout the day in Germany (blue line). Data from 1994 to 2020. The light blue shaded region represents the standard deviation. (b) Comparison of daily distributions on different weekdays, highlighting quantitative differences between weekdays and weekends. (c) Mean daily percentage of individuals using a car (blue line) and standard deviation (shaded region). On weekdays ~55% of the population use a car on average. Data collection for this started in 1999. (d) Variation in daily car usage across different population densities. In rural areas, more than 60% of the population use a car daily, whereas in urban areas, less than 30% do so. The data in question were incorporated into the survey only in the year 2020.

Utilizing the gravity model, we define the traffic flow between an origin o and a destination d using the following equation:

$$F_{od} = \frac{N_o N_d P(t_{od})}{\sum_k N_k P(t_{ok})}, \quad (1)$$

where N_k represents the population at node k , and $P(t_{ok})$ is a function that quantifies the likelihood of a traveler commuting from origin o to node k given the travel time t_{ok} . This assumes that the travel time is the primary influence on commuting decisions, as previously discussed. Henceforward, we will refer to $P(t_{ok})$ as the travel probability function. The above formulation allows us to compute the traffic flow between any pair of origin and destination nodes based on the population sizes and the likelihood of travel under specific travel times.

Next, we estimate the travel probability function. To model this function, we utilize survey data from the MOP that describe the average duration of car trips taken by individuals, which we show in panel (a) of Fig. 3. We have selected a lognormal distribution to fit these data, a choice that is further explained in Appendix A 2. The best-fit of this distribution is depicted by the red line in the figure.

Furthermore, we use the “Global Human Settlement Layer” (GHSL),¹⁷ which provides a spatial raster with a resolution of 100m that represents the distribution of population across the study area. The GHSL achieves these estimates by integrating multiple sources of satellite imagery, census data, and geospatial information to establish a comprehensive global spatial database of human settlements. In the next step, we attribute a population count N_k to each node k . Thereby, we assume that individuals reside solely at junctions, rather than along the roadways. This presumption is necessary to manage

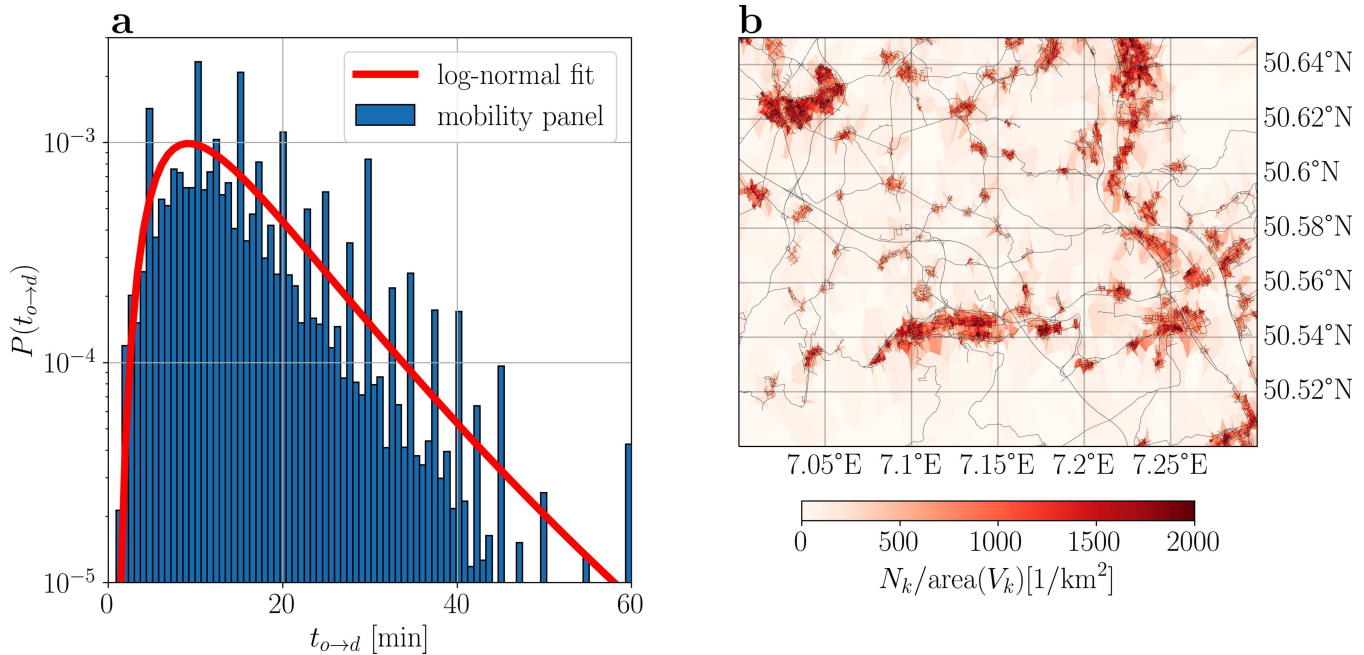


FIG. 3. Travel likelihood data from the “German Mobility Panel” (MOP)¹⁶ and the population density in Bad Neuenahr–Ahrweiler with data taken from the “Global Human Settlement Layer” (GHSL).¹⁷ (a) Travel time data from the MOP shows average duration of car trips taken by individuals for a given time $P(t_{o \rightarrow d})$. The histogram displays the distribution of this data, while the red line represents a lognormal fit. (b) Population density $N_k/\text{area}(W_k)$ in Bad Neuenahr–Ahrweiler using GHSL data. Each node k in the graph is assigned a value based on the size of its corresponding Voronoi polygon W_k , providing an indication of population distribution throughout the area.

the scale of the flow matrix [see Eq. (1)] and, thus, to ensure that the computational demands remain within a practical range for processing. To this end, we calculate the Voronoi polygon W_k for each node k . This polygon represents the area closest to a specific node compared to any other node in the data set. We then determine the population of a node N_k by weighting the intersection of a raster cell W_t from the GHSL data set with the size of the Voronoi polygon W_k associated with a node, such that

$$N_k = \sum_t N_t \frac{\text{area}(W_t \cap W_k)}{\text{area}(W_t)},$$

where N_t is the population of the raster cell. We show the population density of a region in the Ahr valley in panel (b) of Fig. 3.

Furthermore, we define the betweenness of an edge (ij) as the sum of all-pairs shortest paths that pass through that edge,

$$BC_{ij} = \sum_{o,d \in V} \frac{\sigma_{od}(ij)}{\sigma_{od}},$$

where σ_{od} is the number of shortest paths from o to d and $\sigma_{od}(ij)$ is the number of those paths passing through edge (ij).⁵⁰ In a traffic context, the edge betweenness centrality measures how frequently an edge is traversed by commuters if each node had an equal demand and if every commuter always take the shortest path. Hence, it identifies crucial segments that facilitate efficient traffic flow and connectivity between different locations. Thus, it can be viewed as

measure of the importance of roads sections in a transportation network. Previous analyses of the betweenness centrality in urban road networks revealed that it obeys a power law distribution,⁵¹ exhibiting scale-free structures.^{20,52} This suggests that roads are intrinsically ordered in a hierarchical way.

To account for the different intensities of spatial interactions within the network, we integrate the varying demand between nodes o and d , which is given by the flow F_{od} [see Eq. (1)]. This leads to a change in the centrality of edges that are traversed between nodes o and d , in proportion to the magnitude of the traffic flow. By incorporating the traffic flow, we assess how frequently a road (ij) is used. Hence, we define the load of a road L_{ij} as

$$L_{ij} = \sum_{o,d \in V} F_{od} \frac{\sigma_{od}(ij)}{\sigma_{od}}, \quad (2)$$

which is proportional to the number of commuters on the road. The load is also sometimes referred to as spatial interaction incorporated betweenness centrality (SIBC).⁵³ As we sum over the shortest paths in the transportation network, we assume, consistent with our earlier discussion on rational choice theory, that commuters aim to minimize their travel times by selecting the quickest routes available. Additionally, we presume that commuters do not have access to real-time traffic data, which implies that their route choices are made without the benefit of knowing current congestion levels.

Now, we normalize the load values of an edge by the total load

$$\hat{L}_{ij} = L_{ij} / \sum_{(ij) \in E} L_{ij}.$$

We can interpret the normalized load \hat{L}_{ij} as the spatial probability of a commuter being on a specific road (ij). Next, we combine our knowledge of the total population size $N \in \mathbb{N}$ in the region and an estimate of the occupancy rate $\gamma \in [0, 1]$ for a region (which we estimate with respect to the regions population density, compare Fig. 2) to get the number of commuters on a road section. Consequently, the occupancy can be written as

$$\rho_{ij} = \gamma N \hat{L}_{ij}, \tag{3}$$

which yields an estimate of the number of commuters traveling on the roads.

A simulation of the traffic loads in the Ahr valley region can be viewed in panel (a) of Fig. 4. To account for boundary effects, we are simulating a larger region than we are showing in the figure. In Appendix A 3, we show how we select the expanded region. As is to be expected, we find that larger roads such as motorways or federal highways are subject to higher traffic loads than smaller roads. However, as such roads normally have a higher capacity due to more lanes and higher speed limits, this does not necessarily mean that traffic jams occur more often on these roads.

Furthermore, to analyze an effective traffic-related speed reduction, we define the effective velocity $v_{ij,eff} \in [v_{ij,min}, v_{ij,limit}]$ on a road segment, which represents the average speed at which vehicles traverse the segment. This ranges between a minimal velocity that we set to walking speed $v_{ij,min} = 5 \text{ km h}^{-1}$ and a maximal velocity $v_{ij,limit} \in \mathbb{R}$, representing the speed limit of a road.

We describe traffic as a measure of the number of vehicles on a road segment. As such, it is dependent on the length $l_{ij} \in \mathbb{R}$ and the number of lanes $m_{ij} \in \mathbb{N}$ of a road segment, as well as the average

space occupied by a vehicle. Thus, the number of vehicles on ρ_{ij} on a road segment (ij) is determined by the effective velocity of a vehicle multiplied by the reaction time to the vehicle in front $t_r = 2 \text{ s}$ plus the average vehicle length $\bar{d} = 5 \text{ m}$. Therefore, we can further write the occupancy of a road segment as

$$\rho_{ij} = \frac{l_{ij} m_{ij}}{v_{ij,eff} t_r + \bar{d}}. \tag{4}$$

By combing Eqs. (3) and (4), we can compute the effective velocity on a road segment as

$$v_{ij,eff} = \frac{l_{ij} m_{ij}}{\gamma N \hat{L}_{ij} t_r} - \frac{\bar{d}}{t_r} \in [v_{ij,min}, v_{ij,limit}]. \tag{5}$$

This equation for the traffic-related velocities resembles to the equations that employ the density–flow relationship of the Daganzo traffic model.^{13,41,54}

In panel (b) of Fig. 4, we simulate the level of congestion during a peak traffic scenario. For this simulation, we assume an occupancy value of $\gamma = 0.15$, which represents exceptionally high-traffic. Even for this region which has a population density of about $\sim 450 \text{ km}^{-2}$, this value represents congestion levels significantly above the evening rush hour, as depicted in Fig. 2. We selected this occupancy rate because we believe it can represent a realistic outlier scenario of exceptional high traffic, demonstrating that certain sections of the highway experience severe congestion.

D. Imitating congestion by redistributing overloaded road segments

In this section, we present an algorithm aimed at computing the effective velocities, as described in the prior section, in a more realistic way. An issue arises if the occupancy on a road segment exceeds the maximum capacity of the road $C_{ij} \in \mathbb{R}$, that is when the

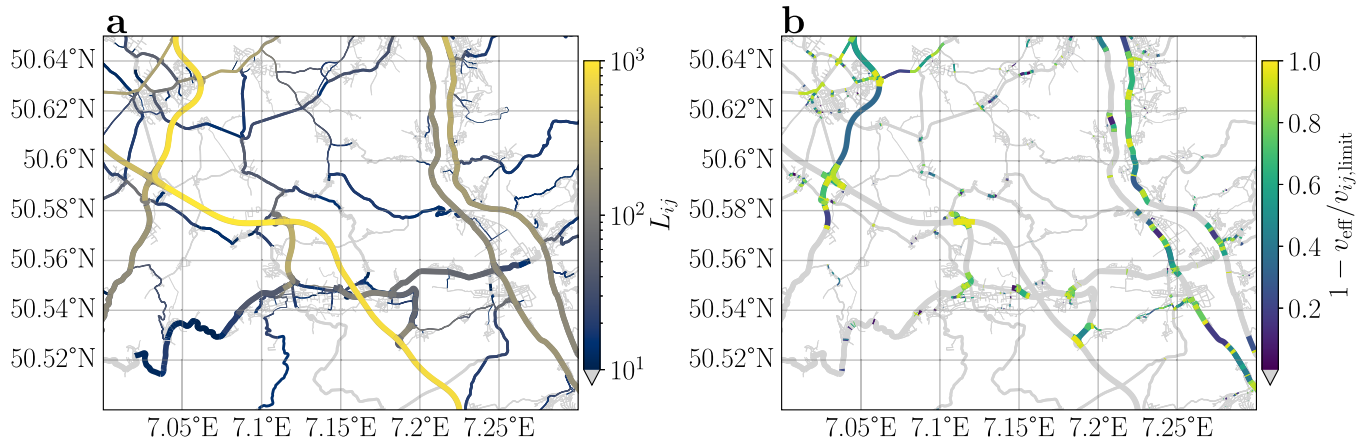


FIG. 4. Simulation of the traffic conditions in the Ahr valley. (a) Using the gravity model of traffic we compute the traffic load L_{ij} of every road in the area around Bad Neuenahr–Ahrweiler and color code it accordingly. To account for boundary effects we simulated the region for a larger area than we are showing, as per Appendix A 3. (b) We compute the effective velocity $v_{ij,eff}$ using Eq. (5) with an occupancy rate of $\gamma = 0.15$, depicting a exceptionally high traffic scenario. With this and the information about the velocity limit we can compute the traffic-related speed reduction $1 - v_{ij,eff} / v_{ij,limit}$ which displays the level of congestion on a road (yellow highly congested, blue lightly congested, light gray no congestion).

ALGORITHM 1. Rerouting excessive traffic in a road network.

```

overloaded_edges = [ ℓ for ℓ in G.edges() if ρℓ > Cℓ ]
while len(overloaded_edges) > 0 do
  for (i, j) in overloaded_edges do
    ΔLij = ρij - Cij
    ρij = ΔLij
    for (n, m) in G.in_edges(i) do
      ρnm + = ΔLij/len(G.in_edges(i))
    end for
  end for
  overloaded_edges = [ ℓ for ℓ in G.edges() if ρℓ > Cℓ ]
end while

```

effective velocity approaches $v_{ij,\min}$. Then, the following condition applies:

$$\rho_{ij} > C_{ij} = \frac{l_{ij}m_{ij}}{v_{ij,\min}t_r + d}.$$

Then, computing the effective velocities as in Eq. (5), we effectively cut off the excess occupancy. We propose redirecting the excess occupancy to previous roads as a solution, as in a real traffic scenario if more vehicles enter a congested road, the congestion will propagate backward. We provide the following algorithm:

The provided algorithm reroutes excessive traffic in a road network. It identifies edges where the current occupancy exceeds the maximum capacity and gradually redistributes the excess occupancy to incoming edges. This process is repeated until no edges have occupancy levels exceeding their capacity, effectively redistributing the traffic load throughout the network such that $\rho_{ij} \leq C_{ij}$. Then, we can use Eq. (5) to calculate the effective velocities and it is ensured that we remain above the lower bound.

In Fig. 5, we provide a visual explanation of how Algorithm 1 works. In panels (a) and (b), we illustrate an example network where an edge is overloaded [this is shown in panel (a)], and we demonstrate how the excess load is rerouted to the previous edges [this is shown in panel (b)]. Furthermore, in panels (c) and (d), we demonstrate the impact of rerouting overloaded roads on a real network. In panel (c), we depict the congestion level obtained when computing the effective velocities according to Eq. (5); panel (d) displays the congestion level after applying the proposed Algorithm 1. It becomes evident that rerouting the excess load significantly affects a substantial portion of the road network. We argue that this approach makes more sense than simply discarding the excess load because, in a real traffic situation, a congestion propagates backward when a road reaches its maximum capacity and more vehicles enter. This is precisely what the proposed Algorithm 1 simulates, capturing the realistic dynamics of traffic flow.

E. Road network reconstruction: Assessing impact and commuter time loss

The resilience of a network typically refers to its capacity to maintain functionality and structure despite experiencing disruptions, like the removal of nodes or edges or other external

perturbations.⁵⁵ There is ongoing effort within the field to discover and apply network structures that can bolster resilience to such disruptions.^{56,57}

In the following analyses, we will examine the resilience of a road network to flood-induced road failures. Here, resilience refers to the ability of the road network to function effectively after a road fails so that the overall traffic flow is impeded as minimally as possible. The focus of our research is on the effective reconstruction of critical roads after a flood disaster. We will find out which roads, after being closed, seriously exacerbate traffic congestion and thus cause bottlenecks. For this purpose, we define the set of failed roads $R \subset E$. To assess the impact of road damage on the network, we compare the intact network, denoted by $G(V, E)$, with the scenario where the roads are destroyed. To achieve this, we remove all edges $\{r_0, r_1, \dots, r_N\} \in R$ from the graph $G(V, E)$, resulting in a modified graph that we designate as $G_r(V, E \setminus R)$. By removing the roads from the graph, we effectively simulate the structural damage inflicted on the road network, allowing us to analyze the consequences to evaluate the network's resilience and robustness in the presence of road failures.

To determine the robustness of the network, we measure how much time commuters lose on all road segments, caused by traffic. To this end, we define commuter time that is calculated by multiplying the time it takes to travel through a road represented by t_{ij} by the number of people passing through that section represented by ρ_{ij} [refer to Eq. (3)]. Hence, we can write the additional commuter time caused by the bridge damage as

$$\Delta T = \sum_{(ij) \in E \setminus R} (\rho_{r,ij}t_{r,ij} - \rho_{ij}t_{ij}). \quad (6)$$

Here, the index r refers to the graph $G_r(V, E \setminus R)$, where road edges have been removed. Subsequently, we can compare different scenarios and evaluate their impact on the overall system. The greater the additional commuter time, the more substantial the impediment to the network's efficacy. In fact, there is also the possibility that the additional commuter time is negative, yielding a net positive effect to the overall traffic. This counterintuitive phenomenon is known as Braess's paradox⁵⁸ and has been found not only in transportation networks but also in other supply networks⁵⁹ such as power grids.^{60,61}

III. RESULTS

In this section, we deploy our method to investigate the effects of the flood disaster in the Ahr valley in July 2021 as a case study. Our investigation focuses on the impact of road and bridge damage on traffic flow and highlights key bottlenecks that have resulted. In addition, we investigate the impact of flooded roads on the accessibility of emergency services. Our analysis shows a significant deterioration in accessibility, particularly in areas adjacent to flooded areas. This investigation highlights not only the vulnerability of infrastructure but also the critical need for strategic emergency planning in such scenarios.

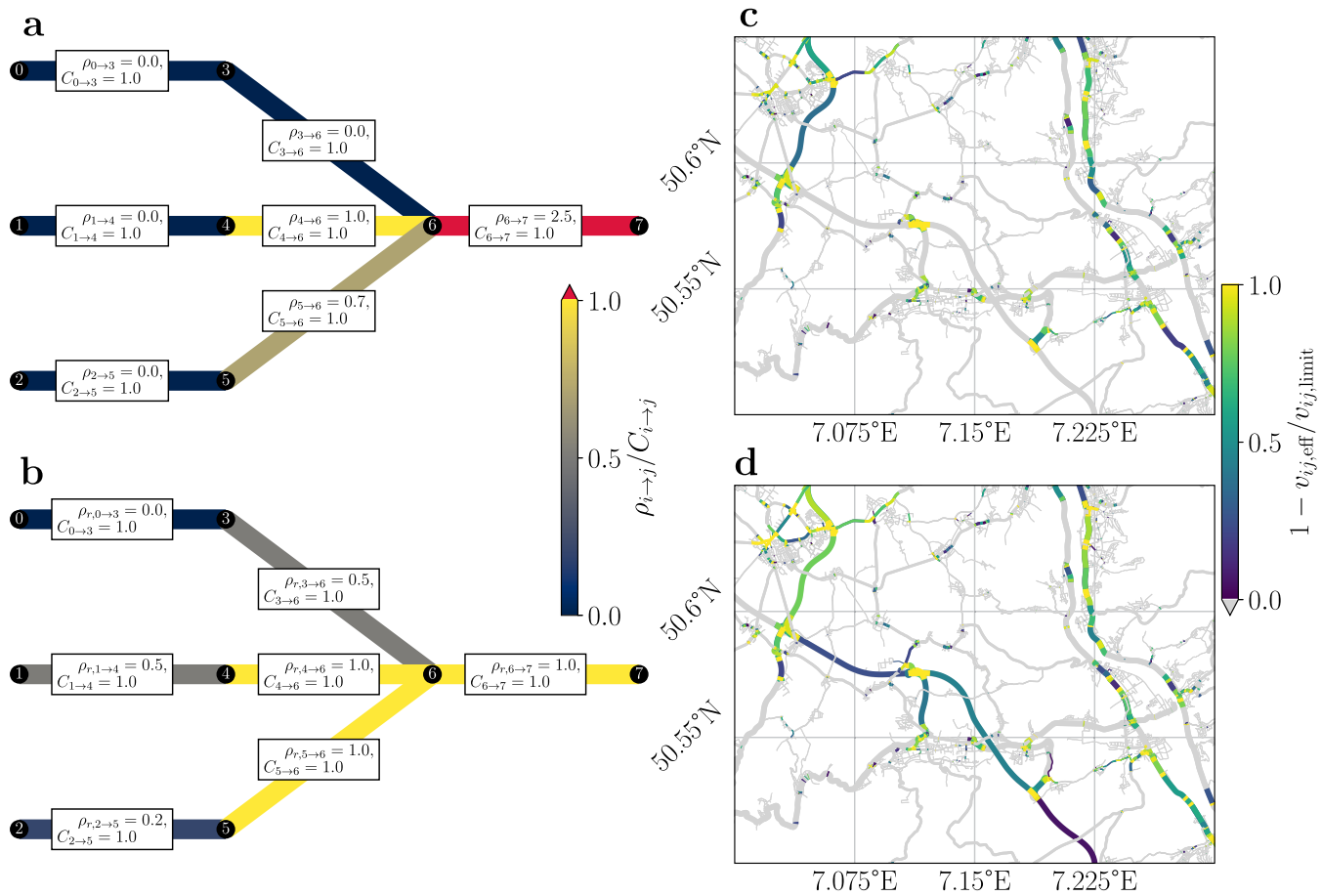


FIG. 5. Visual representation of the redistribution algorithm: When the occupancy ρ_{ij} of a road exceeds its capacity, the excess traffic is redirected to the preceding roads. (a) and (b) We present a toy road network with seven roads and seven intersections/end points to explain Algorithm 1. Each road in the network is assigned a capacity C_{ij} and a occupancy value ρ_{ij} . (a) Initial state of the system, where the occupancy on the edge $\ell = (6 \rightarrow 7)$ surpasses its capacity, is indicated in red. (b) Algorithm 1 redistributes the road occupancy to the preceding roads, effectively rerouting the excess occupancy. In a first step, the excess occupancy of $\Delta\rho_{6 \rightarrow 7} = 1.5$ gets redistributed evenly to the predecessor edges $(3 \rightarrow 6)$, $(4 \rightarrow 6)$, and $(5 \rightarrow 6)$. Then, the edges $(4 \rightarrow 6)$ and the edge $(5 \rightarrow 6)$ exceed their capacity, which in a next step is redistributed to their respective predecessor edges. (c) and (d) Level of congestion (yellow more congested, blue less congested, and light gray no congestion) on a real road networks by illustrating the change of the effective velocities. (c) Effective velocities according to Eq. (5). (d) Effective velocities according to Algorithm 1. In this example, the excess effect is clearly visible as more roads are more heavily congested than in (c).

A. Bridge failures and traffic dynamics: Long-term traffic impairments and prioritization of reconstruction measures

In the aftermath of the flood in the Ahr valley region, bridges, in particular, have experienced substantial and long-term damage. The event resulted in the destruction of a majority of bridges in the area, with most of them remaining impassable for months or replaced with temporary makeshift bridges.⁸ In this section, we aim to analyze the long-term changes in traffic dynamics caused by the inaccessibility of bridges in the Ahr valley.

To capture the potential long-range consequences of the road network disruption, we simulate an area within a 150 km radius

around Bad Neuenahr-Ahrweiler. Then, we set the occupancy rate to $\gamma = 0.1$ to represent a high traffic volume scenario (see Sec. II B).

Furthermore, to optimize computational efficiency, we excluded roads designated as “residential” according to the OSM tagging system. This decision is justified by the significant reduction of the size of the resulting road graph and by the marginal influence that “residential”-roads have on the overall traffic flow, as elaborated in Appendix A 4. Based on our estimates, we assume that approximately 90% of road users are already driving on main roads, while approximately 10% are using roads classified as “residential.” To account for this difference, we adjust the occupancy rate by a factor of 0.9.

Next, we define the set of all bridges $B = \{b_0, b_1, \dots, b_{23}\} \subset E$ that cross the Ahr river in the specified region and remove them from the graph $G(V, E)$, resulting in the modified graph $G_r(V, E \setminus B)$.

To determine the maximum extent of the traffic impacts, we simulate the traffic in the graph without any disruptions $G(V, E)$ and in the graph after the disruption of all bridges $G_r(V, E \setminus B)$. The impact of traffic disruptions is assessed by measuring the change in commuter time, as delineated in Eq. (6) and depicted in panel (a) of Fig. 6. Our analysis reveals that the geographical scope of the impact spans longitudinally from 6.4°E to 8.0°E and latitudinally from 50.1°N to 51.1°N .

Furthermore, we can see in the figure that some roads experience a significant increase in commuter time, while others experience a sharp decrease. This variability can be attributed to the nature of traffic flow dynamics. When a particular road segment is closed, it disrupts the regular flow of vehicles and forces commuters to seek alternative routes. Consequently, adjacent road sections may witness a reduction in traffic volume as they are no longer part of the shortest paths. This alteration in traffic distribution can lead to shorter travel times for these neighboring segments, even in the face of road closures. In fact, the removal of one or more roads may unexpectedly improve the overall traffic conditions, resulting in Braess's paradox.⁵⁸

In this scenario, the closure of the bridges results in a significant deterioration of the traffic flow with a decrease of the commuter time by $\Delta T = 260$ h. This reflects a noticeable decline in the overall

performance of the transportation system. Furthermore, based on the figure, we observe that disruptions in the traffic infrastructure have a significant long-range reach. Here, the traffic restriction extends as far as Cologne, which has a distance of approximately 50 km to the flood's epicenter. This emphasizes the detrimental effect that road failures can have on traffic flow and the commuting experience. It highlights the importance of addressing road maintenance after flood events and of investing in infrastructure improvements to minimize disruptions and ensure a more efficient and reliable transportation network for commuters.

To achieve this, we investigate which bridges have the most significant impact on the stability of the system. Specifically, we aim to identify the bridge that, upon restoration, would yield the most significant decrease in commuter time, thereby optimizing traffic flow and enhancing system efficiency. This information is instrumental in prioritizing bridge rehabilitation projects and allocating resources effectively, with the ultimate goal of minimizing disruptions and optimizing the overall performance of the transportation network.

In panel (b) of Fig. 6, we compare the "null-case," that was discussed previously and is shown in panel (a), where all bridges have failed (indicated by \emptyset), with other scenarios where individual bridges b_k have been restored. We simulate these cases by removing from the graph the bridge edges $B \setminus b_k$, yielding $G_r(V, E \setminus (B \setminus b_k))$. We calculate the total commuter time for each case and compare them. This analysis shows that the bridge b_0 has the greatest

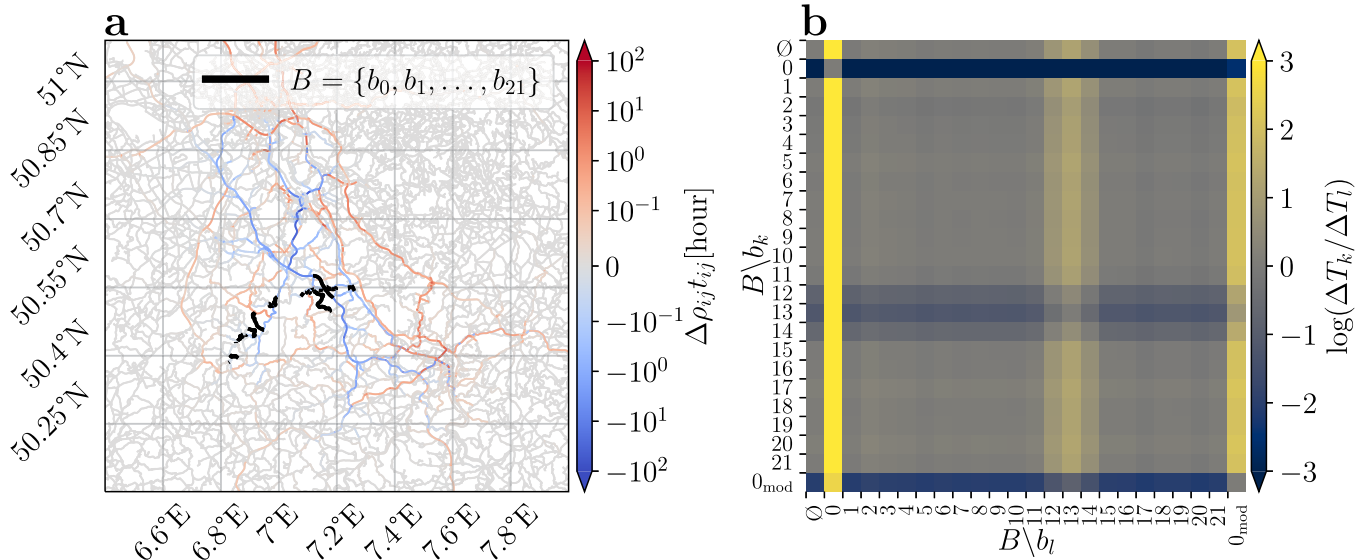


FIG. 6. Impact of bridge losses in the Ahr valley: Analysis of change in commuter time. (a) Representation of failed bridges depicted as thick black lines. We evaluate the traffic flow for an occupancy rate of $\gamma = 0.1$, considering both scenarios with and without the bridges. We assign color to denote the variation in commuter time $\Delta\rho_{ij}t_{ij}$ experienced on each road due to bridge failures. Blue areas indicate reduced commuter time, indicating a decrease in traffic, while red areas signify increased commuter time, reflecting higher traffic levels. The consequences of bridge loss extend to the city of Cologne ($50.9^\circ\text{N} - 51.1^\circ\text{N}$). The cumulative change in commuter time for this particular scenario is estimated as $\Delta T_\emptyset \approx 260$ h. (b) Analysis of individual bridges' impact on cumulative commuter time. We compare two scenarios: the first scenario where all bridges fail [as shown in (a) and in first row/column denoted with \emptyset], and the second scenario where all bridges except one, denoted by b_k , fail. We show the cumulative change in commuter time for each scenario, denoted by ΔT_k . Notably, the bridge labeled as b_0 , corresponding to the bridge on "Bundesstraße 266," exhibits the greatest impact. Therefore, the highest priority for reconstruction should be assigned to this bridge.

impact, as its restoration reduces the commuter time loss to only $\Delta T = 4$ h and thus almost completely restores the pre-flood efficiency of the system. Bridge b_1 is a part of “Bundesstraße 266” (B266), which sustained severe damage during the Ahr river flood. This finding underscores the importance of prioritizing the repair and restoration of the B266 as it has the potential to significantly improve the overall functionality and efficiency of the transportation system, resulting in substantial benefits for commuters.

However, the B266 has been under investigation for some time now due to its relevance to flood risk. Currently, the river has only 30 m of space between the railway tracks of the Ahrtalbahn on the northern bank and the four-lane B266 on the southern bank. During the flood, the water flow through this bottleneck reached $1200 \text{ m}^3 \text{ s}^{-1}$, causing significant damage to the road and railway tracks. By reducing the width of the B266, it is believed that the Ahr river would be able to flow more swiftly during future flood events, with an increased flow volume of approximately $1000 \text{ m}^3 \text{ s}^{-1}$.⁶² However, the B266 is designated as a diversion route in the federal transport infrastructure plan in the event of a blockage on the A61.⁶³ The resulting high impact for the road network stability is captured in our simulation.

In our model, we solely focus on simulating the impact of roads on ensuring smooth traffic flow. However, it is crucial to avoid relying solely on this aspect when making reconstruction plans, as there are various other factors to consider in such decisions. One significant factor to take into account is the potential for significantly improved flood protection and the associated potential for saving lives by narrowing the B266. Consequently, it was recommended not to rebuild the bridge exactly as it was and instead reopen only two out of the former four lanes of the B266.⁶²

In response to this suggestion, we expanded our analysis to include simulations of the specified scenario, which are presented in panel (b) of Fig. 6, specifically in the row and column labeled as 0_{mod} . The results indicate that while the traffic flow is not as optimal as when all lanes are open, there is still a noticeable improvement. Our evaluation indicates that the improvement in commuter time drops to a $\Delta T = 34$ h reduction, in contrast to the $\Delta T = 4$ h achieved with reopening all lanes. Even with this decline, the effect remains substantial, indicating that even with restricted lane availability, there is a noteworthy positive impact on the traffic. Considering the aspect of flood protection, maintaining the functionality of only two out of the four lanes of the B266 emerges as a favorable compromise. This underscores the importance of integrating multiple criteria in the infrastructure planning and disaster preparedness decision-making processes.

B. Effects of flooded roads and traffic on emergency service accessibility

In this section, we analyze the impact of the Ahr flooding on the accessibility of critical emergency services, including ambulances and fire brigades, due to road closures. Our analysis aims to understand the extent to which the flood has affected the ability of these essential services to navigate and reach those in need promptly. We aim to depict a scenario that spans from several days to a few weeks post-flood, during which most or even all roads in the vicinity of the flooding are still inaccessible and restoration

efforts are still under way. It is important to note that this result is not intended to simulate traffic conditions during the flood event itself. Travel behavior during extreme events can deviate significantly from typical patterns,³⁴ a factor that our model does not account for.

To model the accessibility of emergency services, we obtain their locations from OSM and then add them as nodes $S \subset V$ to the graph $G(V, E)$. Then, using Dijkstra’s algorithm⁶⁴ we can compute the distance from every emergency service node to every other node in the network, weighted by effective travel time. This yields information about the emergency service accessibility in different traffic volume scenarios. Here, we assume that emergency vehicles are influenced by traffic just like any other vehicle, which is a simplification as these vehicles theoretically could go for unrestricted travel speeds. Moreover, we also do not account for the formation of emergency lanes by vehicles to allow for unimpeded passage. We argue that the analysis remains justifiable, as the formation of emergency lanes typically does not proceed smoothly⁶⁵ and the results may, therefore, be understood as a worst case scenario.

In the following, we analyze the area that is spanned longitudinally from 6.6°E to 7.5°E and latitudinally from 50.2°N to 50.75°N . The resulting graph, denoted by $G(V, E)$, consists of 42 343 nodes and 101 879 edges. To account for boundary effects, we expanded the simulated area according to Appendix A 3. This allows us to accurately calculate the traffic in the specified region. Furthermore, to analyze the region after the flood event, we define the set of edges R that are intersecting with the flooded area as inaccessible, removing them from the graph $G_r(V, E \setminus R)$.

The response time for emergency vehicles constitutes a crucial planning and quality indicator for the deployment of firefighting and rescue services. It mandates that every incident site located along a public roadway should be accessible within a specified time of travel. The response time specifications vary across federal states, with the Ahr valley located in Rhineland-Palatinate having a response time of 15 min for rescue services and 40 min for ambulance transport.⁶⁶

In Fig. 7, we analyze the feasibility of adhering to the response time in Rhineland-Palatinate and the impact of flood-damaged roads on this indicator. We compare two scenarios [Fig. 7(a)]: non-flooded roads corresponding to the intact graph $G(V, E)$ and flooded roads corresponding to graph $G(V, E \setminus R)$. Furthermore, we analyze how many individuals are not accessible by the fire brigade within a response time frame of $t_r = 15$ min. We examine this number for various occupancy rates $\gamma \in [0, 0.25]$. Our findings indicate that after the flood more than 20 000 people are not accessible within 15 min by the fire brigade at any given moment, even without any traffic. These are the individuals living in the region that is directly affected by the flood. Starting at an occupancy of about $\gamma = 0.1$, the number of those who cannot be reached within a reasonable time increases rapidly.

In panel (b) of Fig. 7, we display the decline in hospital accessibility after the Ahr flooding with an occupancy rate of $\gamma = 0.1$. We simulate traffic in the Ahr valley region, first prior to the flood, to compute the shortest paths from hospitals to other nodes. Then, we simulate traffic again after the flood, excluding flooded roads, and compute the shortest path again. We compute the effective time to reach the closest hospital before and after the flood

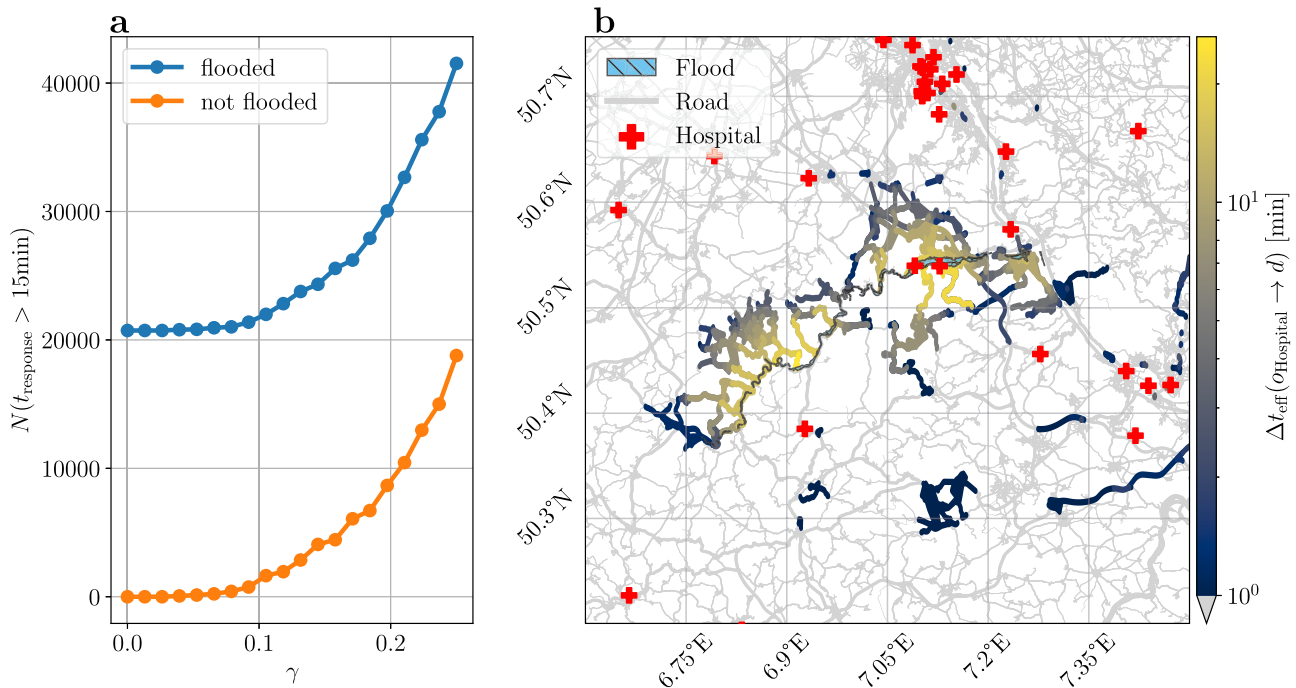


FIG. 7. Impact of flooded roads and traffic on the accessibility of emergency services, including hospitals and fire stations. (a) Two scenarios are considered to analyze the number of individuals N unable to be reached within the emergency response time $t_{\text{response}} = 15$ min at varying road occupancy rates γ . In the first scenario (orange), we show the shortest paths distance from the nearest fire brigade assuming all roads are intact. In the second scenario (blue), the flooded region is simulated by removing affected roads and assessing the resulting accessibility. A significant decline in accessibility is observed at an occupancy level of $\gamma \approx 0.1$, indicating the formation of heavy congestion. (b) Effective travel time from each hospital σ_{Hospital} (red cross signs) to every node d for a occupancy rate of $\gamma = 0.1$ both before and after the flood event (represented by the blue shaded area). Accessibility isochrone polygons (blue areas lightly affected, yellow areas highly affected, gray areas not affected) show the increase of the effective travel time to hospitals, $\Delta t_{\text{eff}}(\sigma_{\text{Hospital}} \rightarrow d)$, caused by flood-induced road damage. The findings reveal a severe impact on the accessibility of hospitals located closer to the flood zone, with an increase of up to approximately 30 min.

and find the time difference $\Delta t_{\text{eff}}(\sigma_{\text{Hospital}} \rightarrow d)$. Subsequently, we construct isochrones originating from each hospital, which are graphical representations of the contour lines on a map indicating areas that can be reached within a specified time interval. The results demonstrate that proximity to the flood event leads to a significant increase, approximately 30 min, in the effective travel time required to reach the closest hospital. Concluding, these results demonstrate that the effects of the flood on the transportation network hinder the accessibility of hospitals drastically.

Based on this analysis, we observe that both the topological loss of roads as well as the traffic conditions hinder the accessibility of emergency services. It becomes evident that a significant proportion of individuals, immediately after the event, may only be reachable through helicopter assistance. In scenarios where accessibility is limited due to traffic congestion, it is critical to educate the public to maintain emergency routes to ensure accessibility.

Efforts should be directed towards promoting public awareness and training initiatives, emphasizing the significance of creating and respecting emergency lanes. Furthermore, it can be a good strategy to keep traffic as low as possible after such events. By doing so, the population can actively contribute to ensuring the availability and accessibility of emergency services in such situations.

IV. DISCUSSION

Disruptive events such as floods reduce the efficiency of the transportation network.¹³ The destruction of roads leads to traffic diversions, resulting in the emergence of bottlenecks. This, in turn, causes the remaining intact roads to become congested, further impeding the smooth flow of traffic. In this paper, we presented a method based on complex networks to analyze the resilience of the transportation networks to such events. As a case study, we applied this method to analyze the impeded transportation network as a consequence of the 2021 flood event in the Ahr valley.

The novelty of our method lies in its consideration of both the altered topological characteristics of the road network and the consequential perturbations to the traffic dynamics. This enables the analysis of indirect effects arising from the redistribution of traffic flow, thereby facilitating a comprehensive examination of the system's behavior. Moreover, an additional strength of this method is that it relies solely on publicly available data, allowing for the analysis of large-scale areas with computational lightweight techniques. However, in this approach that focuses on the broader perspective, limitations arise due to the inability to consider microscopic aspects of traffic.

In this study, we have identified that the disruption of traffic flow in the Ahr valley affects a large area and restricts the efficiency of the transportation system. The effects of this disruption are far-reaching and, in specific traffic scenarios, result in a deterioration of traffic conditions extending up to Cologne, far 50 km from the impact.

We have discovered that the traffic flow can be eased by re-adding specific roads to the system. However, when determining the reconstruction of roads, it is important to consider factors beyond just traffic. In this specific instance, the road in question not only significantly contributes to the overall resilience and efficiency of the road network but also plays a critical role in flood protection. By narrowing the riverbed of the Ahr, this road inadvertently created a bottleneck for the river, which is believed to have contributed to higher damage. Therefore, it was decided to only rebuild only two of the former four lanes.^{62,63}

Our results highlight the necessity of taking into account both the constrained topology of the road network as well as traffic conditions to assess emergency preparedness and response efforts in a comprehensive and reliable way.

We recommend that efforts are focused on promoting public awareness that emphasize the importance of establishing and respecting emergency lanes. Additionally, implementing individual strategies to minimize traffic volume, such as using the bicycle more often, can be beneficial in order to keep the traffic volume low. By taking these steps, we can actively contribute to ensuring the availability and accessibility of emergency services.

We hope that our findings can aid policy makers in prioritizing road restoration and reinforcement initiatives to alleviate the impacts of extreme weather events and thus reducing the likelihood of a chaotic situation akin to the one observed in the Ahr valley.

ACKNOWLEDGMENTS

This research has been funded by the Deutsche Forschungsgemeinschaft (DFG) within the graduate research training group GRK 2043/2 “Natural hazards and risks in a changing world (NatRiskChange)” at the University of Potsdam (Grant No. 251036843).

AUTHOR DECLARATIONS

Conflict of Interest

The authors have no conflicts to disclose.

Author Contributions

Jonas Wassmer: Conceptualization (equal); Data curation (lead); Formal analysis (lead); Methodology (lead); Software (lead); Visualization (lead); Writing – original draft (lead). **Bruno Merz:** Conceptualization (supporting); Methodology (supporting); Supervision (equal); Writing – review & editing (equal). **Norbert Marwan:** Conceptualization (supporting); Methodology (supporting); Project administration (lead); Supervision (equal); Writing – review & editing (equal).

DATA AVAILABILITY

The OSM dump dated 2021-01-02 can be found in OpenStreetMap Data Extracts.²⁹ The GHSL population data set can be found in Schiavina *et al.*¹⁷ The data set from the German Mobility Panel can be found in Ecke *et al.*¹⁶ The satellite image of the flooded area can be found in Copernicus Emergency Management Service.¹⁵ The code used for the analysis and creation of the figures is available at <https://gitlab.pik-potsdam.de/jonaswa/resilience-of-transportation-infrastructure-networks-to-road-failures>.

APPENDIX A: IMPACT OF WEATHER ON VEHICLE USAGE PATTERNS

We analyze the impact of weather conditions to vehicle usage patterns using data from the German Mobility Panel. In Fig. 8, we illustrate the fraction of individuals using a car based on different levels of rainfall and temperature. Panel (a) of the figure shows a clear trend of increasing car usage with rising levels of rainfall. This suggests that people are more likely to opt for the comfort and shelter of a car when the weather is wet. On the other hand, panel (b) shows that car usage remains relatively stable across a range of temperatures, from 2 to 25 °C. This indicates that temperature has a less significant impact on people’s decision to use a car compared to rainfall. The absence of higher temperatures in the data set is attributed to the survey being conducted during the autumn and winter months. A noticeable decline in vehicle users at lower temperatures is observed, which could indicate that people tend to stay at home more at very cold temperatures, but it is important to note that this trend may be influenced by the limited data points available for these temperature ranges, resulting in larger error bars. Therefore, we conclude that temperature has a less significant impact on vehicle usage compared to other factors. In conclusion, we can assert that weather plays a role in influencing mobility patterns. However, in order to make more accurate statements, it would be necessary to conduct the study across different seasons to gather a more comprehensive set of data points.

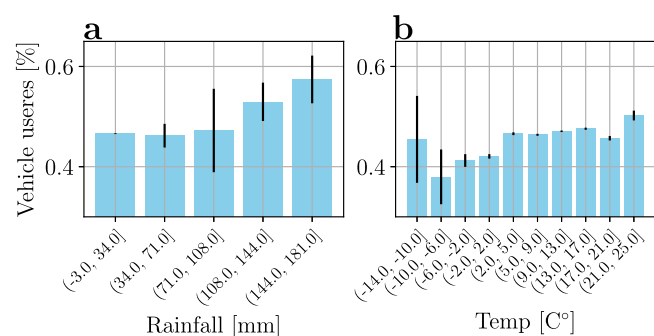


FIG. 8. Fraction of individuals using a car on a day based on (a) rain and (b) temperature values.

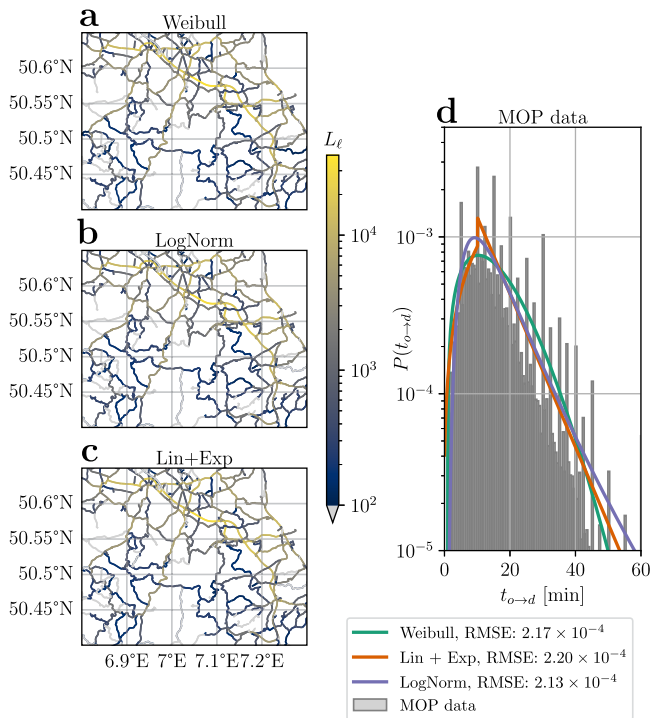


FIG. 9. Load pattern for a region in Germany based on three statistical distributions: Weibull (a), lognormal (b), and a hybrid model with a linear increase followed by exponential decay (c). (d) Travel likelihood data (MOP) with overlaid fits for the three models and their respective RMSE, indicating similar quality fits.

APPENDIX B: STATISTICAL ANALYSIS OF TRIP DISTRIBUTION

We aim to determine the most representative distribution of the travel likelihood in the Mobility Panel [as depicted in panel (d) of Fig. 9]. We explored three statistical distributions: Weibull, lognormal, and a hybrid model combining linear growth with exponential decay.

The adequacy of each distribution was evaluated by calculating the root mean square error (RMSE) between the observed travel patterns and the theoretical predictions. Our analysis revealed negligible differences in the RMSE values, indicating a statistically similar fit among the distributions.

Subsequently, we explored the effect of the selected distribution on traffic load computation. This is visualized through color-coded road graph representations in panels (a)–(c) of Fig. 9, corresponding respectively to the Weibull, lognormal, and the hybrid distributions. The qualitative comparison shows minor variations in the estimated loads across the different models.

To validate these findings, we conducted a comprehensive statistical analysis using 50 randomly selected road graphs from various regions in Germany. This analysis aimed to examine the variability in traffic load predictions derived from each distribution model.

To ascertain the most appropriate distribution for our traffic simulations, we compared the impact of the chosen distribution on

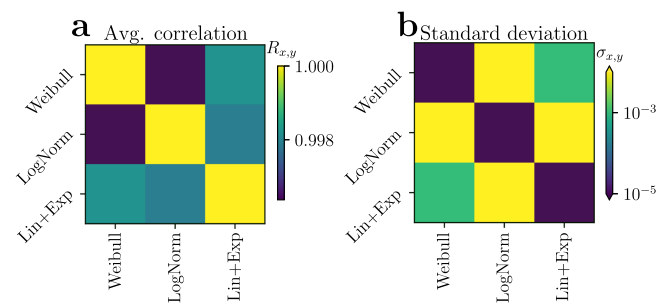


FIG. 10. Correlation matrix analysis of traffic load across three distributions: Weibull (i), lognormal (ii), and linear-exponential hybrid (iii) based on 50 randomly chosen regions in Germany. (a) Averaged correlation matrix of traffic load based on the three distributions. (b) Standard deviations associated with the averaged correlations.

the simulation outcomes. Traffic in 50 randomly selected German regions was simulated using each distribution. A Pearson correlation analysis of the traffic loads [see panel (a) of Fig. 10] demonstrated high correlation and low variability [see panel (b)], suggesting robustness in the simulation results across all distributions.

Despite the hybrid model’s precision, its introduction of a cusp in the distribution led us to discard it. Between Weibull and lognormal, the latter’s tail more closely matched the observed data visually, making the lognormal distribution our choice for this studies simulations.

APPENDIX C: BOUNDARY EFFECTS AND TRAFFIC LOAD CONVERGENCE

To simulate traffic within a specific region, the initial step is to select the area of interest. We denote the respective graph as $G_0(V_0, E_0)$, where V_0 represents the vertices and E_0 represents the edges within the initial region. We then apply Eq. (2) to calculate the traffic load on the roads within the corresponding graph of this region. However, this calculation, if confined to the boundaries of the area, presupposes that all traffic starts and ends within the region, with no vehicles entering or exiting. This assumption does not accurately reflect real-world traffic conditions, which typically span across regional boundaries.

To model traffic dynamics more realistically, we expand the simulation to include an area larger than the initial one. We define the width of this larger graph $G_b(V_b, E_b)$ as the geospatial extent across the graph, ensuring that the width of G_b is greater than the width of G_0 , $\text{width}(G_b) > \text{width}(G_0)$. This expanded graph encompasses traffic that might originate from or be destined for locations outside the initial region.

In this section, we discuss the process for determining the appropriate geospatial width for G_b . The goal is to ensure that the traffic load on any given edge ℓ in E_0 should not be affected by the expansion of the surrounding graph. This requirement is captured by the following condition:

$$\forall \ell \in E_0, \quad \lim_{\text{width}(G_j) \rightarrow \infty} L_\ell^{(G_j)} = L_\ell^{(G_b)}$$

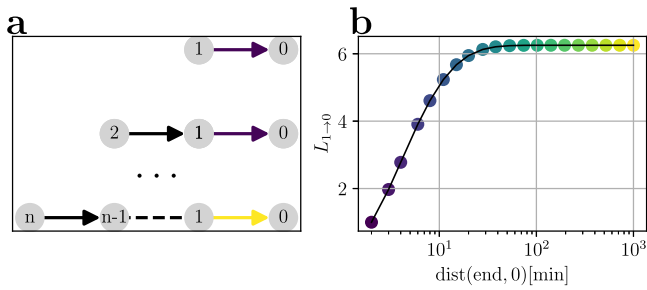


FIG. 11. Illustration of load convergence in a directed path graph. (a) Progressive extension of a directed path graph from 2 nodes to n nodes. (b) Load on the initial edge ($L_{1 \rightarrow 0}$) converges as the path graph expands against the distance from the first to the last node [$\text{dist}(\text{end}, 0)$]. Color coding matches the corresponding edge in panel (a).

Here, $L_\ell^{(G_j)}$ represents the traffic load on edge ℓ within an increasingly larger graphs G_j , indexed by j , and $L_\ell^{(G_b)}$ represents the load on edge ℓ in the extended region, which serves as the benchmark for convergence.

We commence our analysis by examining the load convergence in a simple directed path graph comprising n nodes with uniform population distribution and equal travel time between adjacent nodes. In Fig. 11, we capture this analysis by illustrating the directed path graph's lengthening from 2 to n nodes in panel (a). Next, in panel (b), we plot the load on the right most edge $L_{1 \rightarrow 0}$ against the graph's width, which we here represent by the distance between the first and the last node. We can see that once the distance of the of the first and the last node in the path graph approaches $\text{dist}(\text{end}, 0) \approx 40$ min, the load on the first edge converges to $L_{1 \rightarrow 0} \approx 6$.

To more accurately investigate how the traffic load converges in real road networks, we turn our attention to an actual geographic area in Germany. We begin with a defined square within this region, which serves as the basis for our analysis. This square and the surrounding area are systematically expanded to understand how traffic load behavior changes within the initial confines.

The methodology and results of the traffic load analysis are visually detailed in Fig. 12. Panel (a) outlines the steps involved in constructing traffic graphs for a selected region. Initially, a base graph $G_0(V_0, E_0)$ is formed by enclosing the region of interest within a square. We then systematically expand the square's boundary in 10 km increments, continuing this process until the perimeter extends to 100 km. These stages of expansion are denoted by a series j , where $j \in [10, 20, \dots, 100 \text{ km}]$.

Our next step is to determine when the load on the initial graph G_0 , indicated by $L^{(G_0)}$, reaches convergence. To achieve this, we calculate the loads across all graphs and compare the loads on edges ℓ that are consistent within the expanded and initial graph sets, $\ell \in E_{100 \text{ km}} \cap E_0$, with their corresponding edges in the incrementally expanded graphs, $\ell \in E_j \cap E_0$.

The degree of correlation between the loads of the largest graph and those of the incremental graphs is presented as the Pearson correlation coefficient, $\text{Corr}((L_\ell)^{(G_{100 \text{ km}})}, (L_\ell)^{(G_j)})$, and is depicted in

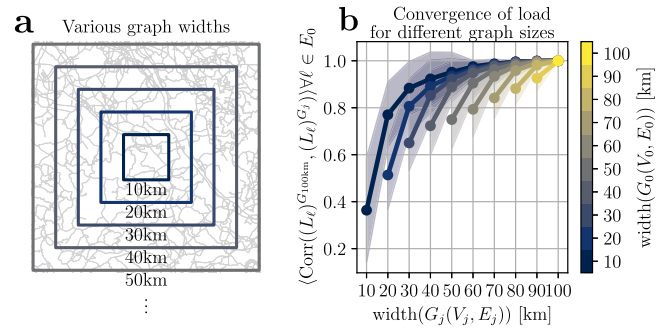


FIG. 12. Illustration of traffic load convergence in incrementally expanded graph widths. (a) Overlay of the road network (in gray) with square perimeters indicating graph boundaries at increasing widths from 10 to 50 km, centered around a focal point. (b) The Pearson correlation coefficient measuring the load convergence of graphs with varying initial widths $G(V_0, E_0)$. Each line, corresponding to a color on the scale from (a), tracks the correlation between the load on edges within the initial graph E_0 and that within expanded graphs of width $G(V_j, E_j)$. The convergence trend is indicated by the Pearson coefficient nearing one as the graph widens. Shaded areas represent the standard deviation, based on comparative data from 50 distinct regions.

panel (b) of Fig. 12. The Pearson correlation approaching the value of one implies that load convergence within the edge set E_0 has been achieved.

For instance, if the initial graph $G_0(V_0, E_0)$ has a width of 10 km (represented by the dark blue line), the load converges when the buffered graph reaches a width close to 50 km. When we repeat the analysis with progressively larger widths for the initial graph—visualized by the color-coded lines—we observe that load convergence occurs earlier for larger initial graph widths. For example, if the initial graph width G_0 is 50 km, the load converges once the buffered graph width(G_j) is at 70 km. This is likely because larger areas tend to retain a greater proportion of the traffic they generate, thus diminishing the impact of the boundaries on overall traffic behavior.

We have extended this analysis to include 50 randomly selected areas across Germany, providing a more comprehensive understanding of the traffic load convergence in varying regional contexts. The average Pearson correlation for these areas is displayed in panel (b) of Fig. 12 as solid lines, offering insight into the general trend of load convergence across different scales. Additionally, the variability in the data is represented by the shaded areas, which denote the standard deviation around the mean correlation values.

APPENDIX D: ROAD CLASSIFICATIONS

Roads that can be used by cars are classified in the OSM database with the tags “motorway,” “motorway_link,” “trunk,” “trunk_link,” “primary,” “primary_link,” “secondary,” “secondary_link,” “tertiary,” “tertiary_link,” “unclassified,” and “residential.” We call a graph that is comprised with these road classes $G(V, E)$.

If we do not include the road tags “residential,” we call the resulting graph $g(v, e)$. We show in panels (a) and (b) of Fig. 13 two

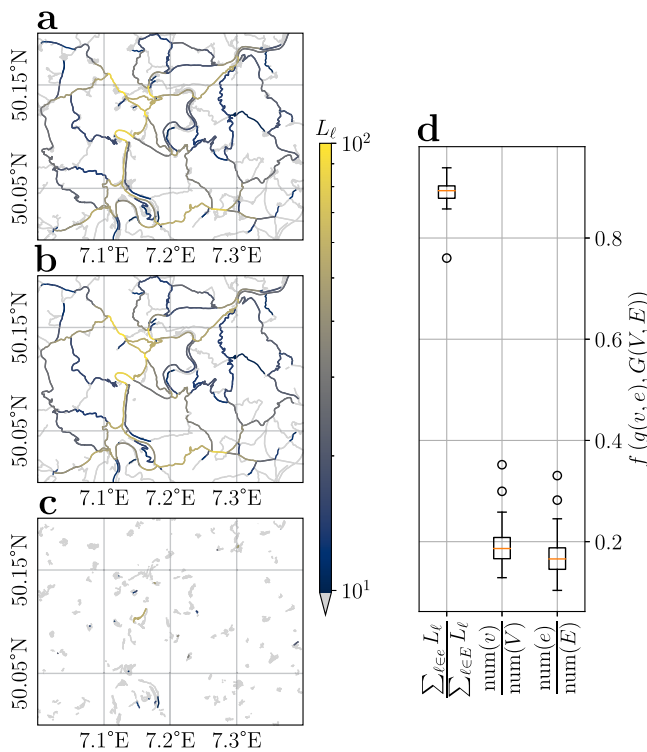


FIG. 13. Comparison of graphs $G(v, e)$ with set of edges E (a) to graphs $g(v, e)$ with set of edges e (b). (a) We show graph $G(V, E)$ which has 3610 nodes v and 9240 edges e . The graph contains the roads classified as “motorway,” “motorway_link,” “trunk,” “trunk_link,” “primary,” “primary_link,” “secondary,” “secondary_link,” “tertiary,” “tertiary_link,” “unclassified,” and “residential.” We compute the loads L_ℓ and color code them. (b) We show the graph $g(v, e)$ which has 554 nodes V and 1186 edges E . In decrement to the road classes listed in (a), the roads classified as “residential” are not included in the graph. Again, we compute the loads L_ℓ and color code them. (c) We show the roads classified as “residential,” $E \setminus e$, and their respective load values. (d) We compare 50 different randomly chosen areas in Germany and show that the average sum of the loads $\sum_{\ell \in e} L_\ell$ divided by the sum of $\sum_{\ell \in E} L_\ell$ is about 0.9. Hence, we conclude that about 90% of commuters are traversing roads classified in (a), and only about 10% are on the additional roads. Moreover, we show that the additional roads increase the number of nodes and edges in the graph 5-fold.

graphs of the same region where the graph in (a) contains the set of edges e yielding a much smaller graph than in (b) which contains the edge set E . We compute the load in both scenarios and argue that they yield qualitatively similar results as about 9/10 of the total sum is distributed on the edge set e . Thus, we argue that roads classified as “residential” are less important for traffic flow than others, since there are fewer vehicles on them. In panel (c), we show a statistical evaluation of our findings, which demonstrates that on average the load on is mostly distributed on the edges e , with only 1/10 of it being on the edges $E \setminus e$. Furthermore, we demonstrate that on average by only including the edges e , the graphs describing the road network is about 5-fold smaller in terms of nodes and edges. Thus, in order to keep the computational load low, in certain applications,

it is useful not to include these roads. However, to do this, we need to adjust the occupancy rate by a factor of 9/10.

APPENDIX E: THE “TRUCK” LANE

On German highways, the right lane is mainly occupied by trucks and is usually crowded on weekdays. Since truck drivers are not included in the mobility statistics, as they are often from abroad, this dynamic is not captured in the simulations. To counteract this, we remove one lane from each edge classified as “motorway” so that $l_{ij, \text{motorway}} = l_{ij, \text{motorway}} - 1$.

REFERENCES

- V. Masson-Delmotte, P. Zhai, A. Pirani, S. L. Connors, C. Péan, S. Berger, N. Caud, Y. Chen, L. Goldfarb, M. Gomis *et al.*, *Contribution of Working Group I to the Sixth Assessment Report of the Intergovernmental Panel on Climate Change* (Cambridge University Press Cambridge, UK, 2021), Vol. 2.
- C. B. Field, “Managing the risks of extreme events and disasters to advance climate change adaptation: Special report of the intergovernmental panel on climate change” (Cambridge University Press, 2012).
- K. C. H. van Ginkel, F. Dottori, L. Alfieri, L. Feyen, and E. E. Koks, *Nat. Hazards Earth Syst. Sci.* **21**, 1011 (2021).
- M. G. Winter, B. Shearer, D. Palmer, D. Peeling, C. Harmer, and J. Sharpe, *Procedia Engineering Advances in Transportation Geotechnics III* (Elsevier, 2016), Vol. 143, p. 1425–1433, 1425 (2016).
- R. Albano, A. Sole, J. Adamowski, and L. Mancusi, *Nat. Hazards Earth Syst. Sci.* **14**, 2847 (2014).
- M. Tsang and D. M. Scott, *J. Transp. Geogr.* **86**, 102774 (2020).
- L. Eiserbeck, see https://www.prognos.com/sites/default/files/2022-07/Prognos_KlimawandelfolgenDeutschland_Detailuntersuchung%20Flut_AP2_3b_.pdf for “Schäden der Sturzfluten und Überschwemmungen im Juli 2021 in Deutschland” (2021) (last accessed on June 13, 2023).
- E. E. Koks, K. C. Van Ginkel, M. J. Van Marle, and A. Lemnitzer, *Nat. Hazards Earth Syst. Sci.* **22**, 3831 (2022).
- J. S. Tradowsky, S. Yi Philip, F. Kreienkamp *et al.*, “Attribution of the heavy rainfall events leading to severe flooding in Western Europe during July 2021,” *Climatic Change* **176**, 90 (2023).
- A. Kermanshah and S. Derrible, *Nat. Hazards* **86**, 151 (2017).
- I. G. Klipper, A. Zipf, and S. Lautenbach, *AGILE GIScience Ser.* **2**, 1 (2021).
- S. Petricola, M. Reinmuth, S. Lautenbach, C. Hatfield, and A. Zipf, *Int. J. Health Geogr.* **21**, 14 (2022).
- A. A. Ganin, M. Kitsak, D. Marchese, J. M. Keisler, T. Seager, and I. Linkov, *Sci. Adv.* **3**, e1701079 (2017).
- OpenStreetMap contributors, see <https://www.openstreetmap.org> for “Planet dump retrieved from <https://planet.osm.org>” (2017).
- Copernicus Emergency Management Service, see <https://emergency.copernicus.eu/mapping/list-of-components/EMSR517> for “Copernicus EMS Rapid Mapping EMSR517: Flood in Western Germany” (2021) (last accessed on June 5, 2023).
- L. Ecke, B. Chlond, M. Magdolen, J. Vallée, and P. Vortisch, “Deutsches mobilitätspanel (MOP) – Wissenschaftliche begleitung und auswertungen bericht 2020/2021: Alltagsmobilität und fahrleistung,” *Technical Report, Karlsruhe Institut für Technologie (KIT)*, 2021.
- M. Schiavina, M. Melchiorri, M. Pesaresi, P. Politis, S. M. Carneiro Freire, L. Maffeni, P. Florio, D. Ehrlich, K. Goch, P. Tommasi, and T. Kemper, *GHSL data package 2022* (Publications Office of the European Union, Luxembourg, 2022).
- M. Barthélemy and A. Flammini, *J. Stat. Mech.: Theory Exp.* **2006**, L07002 (2006).
- D. J. Aldous, *J. Stat. Mech.: Theory Exp.* **2008**, P03006 (2008).
- M. Barthélemy, *Phys. Rep.* **499**, 1 (2011).
- G. Boeing, *Appl. Network Sci.* **4**, 1 (2019).
- G. Boeing, *Environ. Plann. B* **47**, 590 (2020).
- C. Ludwig, S. Lautenbach, E.-M. Schömann, and A. Zipf, in *11th International Conference on Geographic Information Science (GIScience 2021)—Part II*, Leibniz

International Proceedings in Informatics (LIPIcs) Vol. 208, edited by K. Janowicz and J. A. Versteegen (Schloss Dagstuhl – Leibniz-Zentrum für Informatik, Dagstuhl, 2021), pp. 3:1–3:15.

- ²⁴L. Zhang and D. Pfoser, *PLoS One* **14**, e0212606 (2019).
- ²⁵P. Neis, P. Singler, and A. Zipf, “Collaborative mapping and emergency routing for disaster logistics—Case studies from the Haiti earthquake and the UN portal for Afrika” (2023).
- ²⁶S. Scholz, P. Knight, M. Eckle, S. Marx, and A. Zipf, *Remote Sens.* **10**, 1239 (2018).
- ²⁷P. Lopes, C. Fonte, L. See, and B. Bechtel, in *2017 Joint Urban Remote Sensing Event (JURSE)* (IEEE, 2017), pp. 1–4.
- ²⁸M. Schultz, J. Voss, M. Auer, S. Carter, and A. Zipf, *Int. J. Appl. Earth Obs. Geoinf.* **63**, 206 (2017).
- ²⁹Geofabrik GmbH, see <https://download.geofabrik.de/> for “Geofabrik—OpenStreetMap Data Extracts” (2023) (last accessed June 30, 2023).
- ³⁰J. Topf, see <https://osmcode.org/osmium-tool/> for “Osmium: A Multipurpose Command Line Tool for Working with OpenStreetMap Data” (2010).
- ³¹G. Boeing, *Comput. Environ. Urban Syst.* **65**, 126 (2017).
- ³²E. Martínez-Gomariz, M. Gómez, B. Russo, and S. Djordjević, *Urban Water J.* **14**, 930 (2017).
- ³³F. J. Shahdani, M. Santamaria-Ariza, H. S. Sousa, M. Coelho, and J. C. Matos, *Appl. Sci.* **12**, 3076 (2022).
- ³⁴J. Tang, P. Zhao, Z. Gong, H. Zhao, F. Huang, J. Li, Z. Chen, L. Yu, and J. Chen, *Natl. Sci. Rev.* **10**(8), nwad097 (2023).
- ³⁵M. C. Gonzalez, C. A. Hidalgo, and A.-L. Barabasi, *Nature* **453**, 779 (2008).
- ³⁶A. Lima, R. Stanojevic, D. Papagiannaki, P. Rodriguez, and M. C. Gonzalez, *J. Royal Soc. Interface* **13**, 20160021 (2016).
- ³⁷S. Batista, L. Leclercq, and N. Geroliminis, *Transp. Res. Part B Methodol.* **122**, 192 (2019).
- ³⁸S. Zhu and D. Levinson, *PLoS One* **10**, 0134322 (2015).
- ³⁹H. G. Ramirez, L. Leclercq, N. Chiabaut, C. Becarie, and J. Krug, *Travel Behav. Soc.* **22**, 59 (2021).
- ⁴⁰J. G. Wardrop and J. I. Whitehead, *Proc. Inst. Civil Eng.* **1**, 767 (1952).
- ⁴¹Z. Chen, C. Yang, J.-H. Qian, D. Han, and Y.-G. Ma, *Chaos* **33**, 033132 (2023).
- ⁴²S. L. Green, in *Baylor University Faculty Development Seminar on Rational Choice Theory* (Baylor University, Waco, TX, 2002), pp. 1–72.
- ⁴³P. H. Bovy and E. Stern, *Route Choice: Wayfinding in Transport Networks: Wayfinding in Transport Networks* (Springer Science & Business Media, 2012), Vol. 9.
- ⁴⁴J. Nguyen, S. T. Powers, N. Urquhart, T. Farrenkopf, and M. Guckert, *Transp. Res. Interdiscip. Perspect.* **12**, 100486 (2021).
- ⁴⁵G. K. Zipf, *American Sociological Review* **11**, 677 (1946).
- ⁴⁶A. M. Voorhees, *Transportation* **40**, 1105 (2013).
- ⁴⁷W.-S. Jung, F. Wang, and H. E. Stanley, *Europhys. Lett.* **81**, 48005 (2008).
- ⁴⁸G. Cheng, C. G. Wilmot, and E. J. Baker, *Transp. Res. Res. J. Transp. Res. Board* **2234**, 125 (2011).
- ⁴⁹M. F. Guagliardo, *Int. J. Health Geogr.* **3**, 3 (2004).
- ⁵⁰L. C. Freeman, *Sociometry* **40**(1), 35 (1977).
- ⁵¹S. Lämmer, B. Gehlsen, and D. Helbing, *Phys. A* **363**, 89 (2006).
- ⁵²A.-L. Barabási and E. Bonabeau, *Sci. Am.* **288**, 60 (2003).
- ⁵³X. Wu, W. Cao, J. Wang, Y. Zhang, W. Yang, and Y. Liu, *PLoS One* **17**, e0268203 (2022).
- ⁵⁴C. F. Daganzo, *Transp. Res. Part B Methodol.* **28**, 269 (1994).
- ⁵⁵J. Gao, B. Barzel, and A.-L. Barabási, *Nature* **530**, 307 (2016).
- ⁵⁶F. Kaiser, V. Latora, and D. Witthaut, *Nat. Commun.* **12**, 3143 (2021).
- ⁵⁷J. Wassmer, D. Witthaut, and F. Kaiser, *J. Phys. Complexity* **2**, 035003 (2021).
- ⁵⁸D. Braess, *Unternehmensforschung* **12**, 258 (1968).
- ⁵⁹D. Manik, D. Witthaut, and M. Timme, *arXiv:2205.14685* (2022).
- ⁶⁰D. Witthaut and M. Timme, *New J. Phys.* **14**, 083036 (2012).
- ⁶¹B. Schäfer, T. Pesch, D. Manik, J. Gollenstede, G. Lin, H.-P. Beck, D. Witthaut, and M. Timme, *Nat. Commun.* **13**, 5396 (2022).
- ⁶²T. Weber, see https://ga.de/region/ahr-und-rhein/bad-neuenahr-ahrweiler/flut-arbeitsgruppe-fordert-rueckbau-der-b-266-bei-heimersheim_aid-73185473 for “Flut-arbeitsgruppe fordert rückbau der b266 bei heimersheim” (2022) (last accessed June 12, 2023).
- ⁶³M. Gärtner, see <https://www.swr.de/swraktuell/rheinland-pfalz/koblenz/b266-nach-flutkatastrophe-nicht-aufbauen-heimersheim-100.html> for “Mehr platz für die ahr bei heimersheim: B266 soll schmaler werden” (2022) (last accessed June 12, 2023).
- ⁶⁴E. W. Dijkstra, *Numer. Math.* **1**, 269 (1959).
- ⁶⁵D. R. Kreuz, see <https://www.drk.de/presse/pressemitteilungen/meldung/in-80-prozent-aller-faelle-funktioniert-die-rettungsgasse-nicht-richtig/> for “In 80 prozent aller fälle funktioniert die rettungsgasse nicht richtig” (2018) (last accessed June 14, 2023).
- ⁶⁶L. Rheinland-Pfalz, see https://mdi.rlp.de/fileadmin/03/Themen/Bevoelkerungsschutz_und_Rettungsdienst/Rettungsdienst/Dokumente/2624-Landesrettungsdienstplan_2023.pdf for “Rettungsdienst Landesrettungsdienstplan Rheinland-Pfalz (LRettDP)” (2008) (last accessed June 7, 2023).